ELSEVIER

Chemical Engineering Journal 133 (2007) 165–172

Chemical Engineering Journal

www.elsevier.com/locate/cej

A rate based reactor model for BiodeNOx absorber units

J.G.M. Winkelman, F. Gambardella, H.J. Heeres *

Department of Chemical Engineering, Stratingh Institute, RijksUniversiteit Groningen, Nijenborgh 4, 9747 AG Groningen, The Netherlands

Received 24 November 2005; received in revised form 21 February 2007; accepted 1 March 2007

Abstract

The reactive absorption of NO in aqueous solutions of Fe^{II}(EDTA), resulting in the formation of a nitrosyl complex, Fe^{II}(EDTA)(NO), is a key step of the BiodeNOx process for the removal of NOx from industrial flue gas. Oxygen present in the flue gas will also absorb and oxidize Fe^{II}(EDTA). This is an undesired reaction, because the resulting Fe^{III}(EDTA) does not react with NO. To explore the industrial applicability of the process, a rate based model for the simultaneous reactive absorption of NO and O_2 in aqueous Fe^{II}(EDTA) solutions in a counter current packed column has been developed. The effect of process conditions on absorber performance (NO removal efficiency, selectivity, Fe^{II}(EDTA) conversion) have been assessed. Using standard conditions, the column height needed to remove 90% of an initial 250 ppm of NO was less than 1 m. The amount of oxidized iron was approximately equal to the amount of the nitrosyl complex, even though oxygen was present in a 200-fold excess over NO. The absorber performance was particularly dependent on the operating temperature, where lower temperatures favoured both the NO removal efficiency and selectivity. Remarkably, the model indicated that overdesign of the absorber can result in decreasing absorber performance.

Keywords: NO Absorption; BiodeNOx; Reactor modeling

1. Introduction

Atmospheric emission of NOx causes various environmental problems, such as an increase in ground-level ozone, smog and acid rain formation, and the depletion of the ozone layer. A promising technique for the removal of NOx from industrial flue gas is the BiodeNOx process. It consists of two discrete stages: in a first, physico-chemical stage NO is absorbed into an aqueous iron chelate solution, and in a second, biological stage the iron chelate is regenerated while at the same time NO is converted to harmless nitrogen [1].

In the absorber section, the absorption of NO is accompanied by a rapid reversible reaction of NO with the iron chelate in the solution. This way, both the NO absorption rate and capacity of the solution to accommodate NO are greatly increased. If ethylene diamine tetracetic acid, EDTA, is used as the chelating component, nitrosyl complex formation can be written as

$$Fe^{II}(EDTA)^{2-} + NO \rightleftarrows Fe^{II}(EDTA)(NO)^{2-} \quad (1)$$

In general, industrial flue gases contain molecular oxygen, typically in amounts ranging from 2% to 10%. Dissolved oxygen also reacts with the iron chelate, where the ferrous chelate is oxidized irreversibly to ferric chelate according to

$$O_2 + 4Fe^{II}(EDTA)^{2-} + 2H_2O \rightarrow 4Fe^{III}(EDTA)^{-} + 4OH^{-} \quad (2)$$

In its ferric form, Fe^{III}(EDTA) can no longer bind NO. Thus, the oxidation according to reaction (2) is an unwanted side reaction since it consumes Fe^{II}(EDTA) that is needed for NO absorption. Additionally, the work load of the second, biological stage of the BiodeNOx process increases, because Fe^{II}(EDTA) has to be recovered not only from the nitrosyl complex via reduction of NO to N_2, but also from ferric chelate via reduction of Fe^{III}(EDTA).

A typical flue gas from a coal-fired power plant can contain, say, 250 ppm NO and 5% O_2. In such a (realistic) case the oxygen concentration in the gas exceeds the NO concentration 200-fold. Thus, for any practical application of the BiodeNOx process, it becomes very important to assess the extent of the unwanted oxidation reaction (2) as compared to the desired reaction (1) in a typical absorber.

In this contribution we present a model for the performance of BiodeNOx absorbers based on the results of previous studies on various aspects of the BiodeNOx absorption process [2–5]. The main objectives are to investigate the absorber dimensions

* Corresponding author. Fax: +31 50 363 4479.
E-mail address: h.j.heeres@rug.nl (H.J. Heeres).

1385-8947/$ – see front matter © 2007 Elsevier B.V. All rights reserved.
doi:10.1016/j.cej.2007.03.002

Nomenclature

A	nitric oxide NO
a	interfacial area, $m^2\ m^{-3}$
a_P	geometric area of packing, $m^2\ m^{-3}$
B	ferrous iron chelate $Fe^{II}(EDTA)^{2-}$
C	concentration, $mol\ m^{-3}$ or vppm
D	diffusion coefficient, $m^2\ s^{-1}$
d_P	characteristic packing dimension, m
E	enhancement factor
F	molar flow, $mol\ s^{-1}$
F_P	packing factor, $m^2\ m^{-3}$
g	gravitational acceleration = $9.81\ m^2\ s^{-1}$
J	flux of absorption, $mol\ m^{-2}\ s^{-1}$
k	mass transfer coefficient, $m\ s^{-1}$
k_2	kinetic constant for the oxygen absorption, $m^6\ mol^{-2}\ s^{-1}$
O	oxygen
P	nitrosyl complex $Fe^{II}(EDTA)(NO)^{2-}$
Q	ferric iron chelate $Fe^{III}(EDTA)^{-}$
r_1, r_2	reaction rates, see Eqs. (7)–(8), $mol\ m^{-3}\ s^{-1}$
S	cross-sectional reactor area, m^2
V_S	superficial velocity, $m\ s^{-1}$
X_B	conversion of $Fe^{II}(EDTA)^{2-}$

Greek symbols

ε_L	liquid hold-up
η	efficiency
μ	viscosity, Pa s
ρ	density, $kg\ m^{-3}$
σ	selectivity

Subscripts

G	gas phase
L	liquid phase

Superscripts

b	bulk
i	interface
in	inlet
out	outlet

needed to obtain a desired NO removal efficiency and the feasibility of the NO removal in the presence of relatively large oxygen excess concentrations. The influence of the operating temperature and the iron chelate concentration on the absorber performance are also investigated.

2. Model development

Various reactor configurations for reactive gas–liquid absorption have been developed and commercialized. We have selected a counter current packed tower absorber for our modeling study. This reactor appears to be particularly appropriate for the Biode-NOx process as it offers a high interfacial area, and is capable of handling high gas superficial velocities with a low pressure drop.

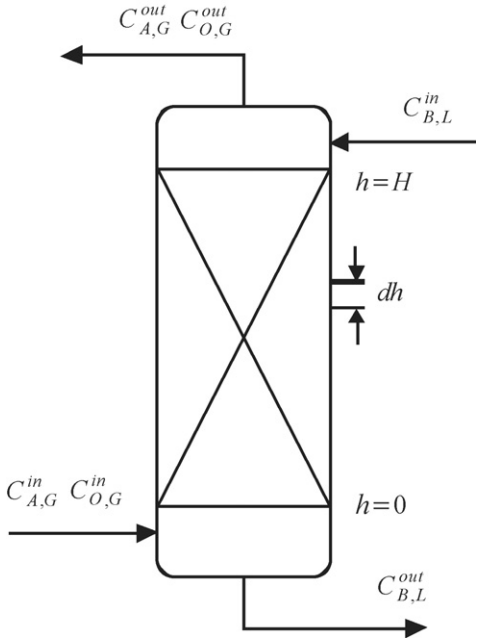

Fig. 1. Packed column reactor configuration.

A representation of the reactor configuration is given in Fig. 1. A gas mixture containing NO and oxygen is fed at the bottom of the column. The aqueous phase containing $Fe^{II}(EDTA)$ is fed to the top of the column.

The gas phase component balances, assuming plug flow, read:

$$V_{S,G}\frac{dC_{n,G}}{dh} = -J_{n,G}a \quad (n = A, O) \tag{3}$$

where $J_{n,G}$ is the absorption flux of NO (A) or oxygen (O) through the gas liquid interface (see Fig. 2), with the positive direction from the gas towards the liquid. The boundary conditions to Eq. (3) simply state that at the bottom of the column, the gas phase concentrations equal the gas feed concentrations:

$$(C_{n,G})_{h=0} = C^{in}_{n,G} \quad (n = A, O) \tag{4}$$

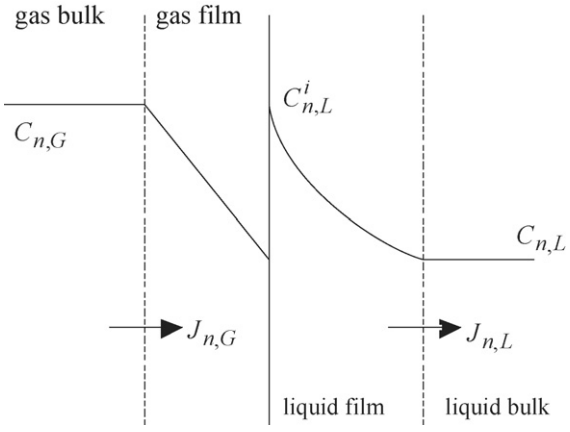

Fig. 2. Mass transfer fluxes and generalized profiles according to the film model.

For the liquid bulk, we have the balances:

$$V_{S,L}\frac{dC_{n,L}}{dh} = -J_{n,L}a + \varepsilon_L R_{n,L} \quad (n = A, O, B, P, Q) \tag{5}$$

where $J_{n,L}$ denotes the diffusion flux from the interface region into the liquid bulk (see Fig. 2) with the positive direction towards the bulk. $R_{n,L}$ denotes the reaction rate in the liquid bulk, positive for the reactants A, O and B (ferrous chelate) negative for the reaction products P (nitrosyl complex) and Q (ferric chelate), and ε_L denotes the liquid hold-up in the packed bed.

The boundary conditions to Eq. (5) relate the liquid phase concentrations at the top of the column to the liquid feed concentrations:

$$(C_{n,L})_{h=H} = C_{n,L}^{in} \quad (n = A, O, B, P, Q) \tag{6}$$

The system of Eqs. (3)–(6) constitutes a two-point boundary value problem and was solved using a relaxation method. The equations contain the fluxes $J_{n,L}$ and $J_{n,G}$.These fluxes are related to the concentration gradients in the gas and liquid film layers (see Fig. 2) and were calculated numerically.

3. Calculation of the fluxes

In the scrubber, we have absorption of NO (A) and oxygen (O) across the gas liquid interface. In the liquid, the diffusive transport is accompanied by chemical reactions, according to reactions (1) and (2). The rates of reactions (1) and (2) are given by [2,3]:

$$r_1 = k_1\left(C_A C_B - \frac{C_P}{K}\right) \tag{7}$$

$$r_2 = k_2 C_O C_B^2 \tag{8}$$

According to the film model, see Fig. 2, the material balances for diffusion with parallel reaction in the liquid film read [6]:

$$D_A\frac{d^2C_A}{dx^2} = R_A = r_1 \quad (0 \le x \le \delta) \tag{9}$$

$$D_O\frac{d^2C_O}{dx^2} = R_O = r_2 \quad (0 \le x \le \delta) \tag{10}$$

$$D_B\frac{d^2C_B}{dx^2} = R_B = r_1 + 4r_2 \quad (0 \le x \le \delta) \tag{11}$$

$$D_P\frac{d^2C_P}{dx^2} = R_P = -r_1 \quad (0 \le x \le \delta) \tag{12}$$

$$D_Q\frac{d^2C_Q}{dx^2} = R_Q = -4r_2 \quad (0 \le x \le \delta) \tag{13}$$

The boundary condition at the liquid bulk side of the film reads for all components:

$$(C_n)_{x=\delta} = C_{n,L} \tag{14}$$

where $C_{n,L}$ denotes the liquid bulk concentration in the absorber at the height where the fluxes are calculated. At the interface, a distinction is made between transferable and non-transferable components. For the dissolved gases the interface condition reads:

$$-D_n\left(\frac{dC_n}{dx}\right)_{x=0} = k_{G,n}\left(C_{n,G} - \frac{(C_n)_{x=0}}{m_n}\right) \quad (n = A, O) \tag{15}$$

while for non-transferable components we have:

$$\left(\frac{dC_n}{dx}\right)_{x=0} = 0 \quad (n = B, P, Q) \tag{16}$$

For the fluxes across the gas liquid interface we have:

$$J_{n,G} = k_{G,n}\left(C_{n,G} - \frac{C_{n,L}^i}{m_n}\right) \quad (n = A, O) \tag{17}$$

and for the fluxes from the liquid film into the liquid bulk at $x = \delta$:

$$J_{n,L} = -D_n\left(\frac{dC_n}{dx}\right)_{x=\delta} \quad (n = A, O, B, P, Q) \tag{18}$$

The concentration profiles of the components were calculated by solving the system of Eqs. (9)–(13), using a relaxation method to obtain finite difference equations and solving the system with the method of Newton. Subsequently, the fluxes were calculated using Eqs. (17) and (18). To obtain the gradient of the concentration at $x = \delta$, a Taylor series expansion of the corresponding concentration was used.

4. Physico-chemical constants and model parameters

The nitrosyl complex formation reaction, Eq. (1), is first order in the substrates and the product. The rate of the reaction was measured by Schneppensieper et al. [7]. The equilibrium constant for the reaction as a function of the temperature was measured previously in our group work [2] as

$$K = \exp\left(\frac{4702}{T} - 8.53\right)(m^3/mol) \tag{19}$$

All kinetic studies concerning the oxidation reaction (2) indicate that the reaction is first order in oxygen. However, the order in iron chelate appears to be more complex and values between 1 and 2 have been reported [8–10]. Recent studies have indicated that the order in iron is a function of the iron chelate concentration [11,12]. At low concentrations ($\ll 10\,mol/m^3$), the reaction is first order in iron whereas it becomes second order at higher concentrations. At typical BiodeNOx absorption conditions ($T = 50$–$55\,^\circ C$, $C_{FeII(EDTA)} = 10$–$50\,mol/m^3$, $C_{NO} = 0$–$250\,vppm$, $C_{O_2} = 10$–20%, pH 7), the reaction was shown to be first order in oxygen and second order in iron chelate [3], as shown in the rate given by Eq. (8). The rate constant for the oxidation reaction as a function of the temperature was measured previously in our group and may be expressed as [3]:

$$k_2 = \exp\left(10.156 - \frac{4615.4}{T}\right)(m^6/mol^2\,s) \tag{20}$$

where no significant variation of k_2 was observed in the pH range of 5–8. This is in line with the observations of Zang and Van Eldik [11], who measured k_2 in the pH range of 1–7, and found no variation of k_2 for pH ≥ 5 while increased values were found for pH ≤ 4. In the calculations we assumed that acidic gaseous components that could be present in the gas feed do not lower the pH below 4.5, so we can safely use Eq. (20) to obtain k_2.

The diffusion coefficient of NO in water is given by Wise and Houghton [13]. The diffusion coefficient of oxygen in Fe^{II}(EDTA) solutions at various concentrations was calculated using the diffusivity of oxygen in water [14] and corrected for the presence of electrolytes [15]. The diffusion coefficients of the iron chelate, D_B, was taken from O'Conner et al. [16]. The diffusion coefficients of NO and oxygen in the gas phase were calculated using an expression given by Reid et al. [17]. The viscosity of the gas phase was assumed to be equal to the viscosity of N_2, which is given by Daubert and Danner [18].

The solubilities of NO and O_2 in Fe^{II}(EDTA) solutions were determined from physical absorption experiments using N_2O and the results are reported in previous papers of our group [2,3]. We also measured the relative viscosity and the density of the aqueous Fe^{II}(EDTA) solutions at various concentrations and temperatures. The results were published earlier [5].

An overview of the physical constants obtained at a temperature of 323 K and an iron chelate concentration of 10 mol/m^3 is given in Table 1.

Many types of so-called random packing materials are commercially available. From a technical point of view, based on a trade off between on the one hand the desire for a low-pressure drop, leading to larger packing material diameters, and on the other hand the benefits of a large surface area, pointing at smaller packing diameters, we chose to perform the modeling calculations using the properties of 1 in. Pall rings.

The mass transfer coefficients in the column were estimated using the well-known equations of Onda et al. [19,20]. The surface area, packing factor, packing dimensions, flooding limits, minimum wetting flow rate of the liquid, and the pressure drop were obtained or calculated from the data and expressions given by Trambouze et al. [21]. The liquid hold-up in the column was calculated according to Buchanan [22].

Table 1
Overview of physical constants at $T = 323$ K and $C_{FeII(EDTA)} = 10$ mol/m^3

Parameter	Value
$D_{NO,L}$ (m^2/s)	8.65×10^{-9}
$D_{O_2,L}$ (m^2/s)	4.07×10^{-9}
$D_{FeII(EDTA),L}$ (m^2/s)	1.08×10^{-9}
$D_{NO,G}$ (m^2/s)	2.79×10^{-5}
$D_{O_2,G}$ (m^2/s)	2.40×10^{-5}
He_{NO} (Pa m^3/mol)	7.2×10^4
He_{O2} (Pa m^3/mol)	1.08×10^5
$\mu_{FeII(EDTA)}/\mu_W$	1.02
$\rho_{FeII(EDTA)}$ (kg/m^3)	992

5. Results and discussion

5.1. Definition base case and results

The reactor model is developed for the treatment of a typical flue gas of a coal-fired power plant. The oxygen concentration in the flue gas was set at 5 vol.% and the NO concentration at 250 vppm. The temperature of the flue gas and the operating temperature of the absorber, in the base case, were set at 323 K. The desired removal efficiency for NO was 90%. The input concentrations, process conditions and design variables for the base case are given in Table 2. Typical superficial gas and liquid velocities for packed columns were applied. The liquid velocity was set to guarantee full wetting of the packing. The gas phase velocity was always typically between 55% and 60% of the flooding value. The pressure drop for the base case is 290 Pa.

The inlet iron chelate concentration was selected on the basis of earlier simultaneous absorption studies of NO and O_2 in Fe^{II}(EDTA) solutions in a stirred cell reactor [4].

Model calculations for the base case indicate that a column height of 0.91 m is required to obtain 90% NO removal efficiency. The total iron chelate conversion, X_B, in the absorber is about 6.3%.

The calculated selectivity of the gas absorption, as defined in Eq. (21), is equal to 45% for the base case, meaning that 45% of the Fe^{II}(EDTA) is converted to Fe^{II}(EDTA)(NO) and 55% is oxidized to Fe^{III}(EDTA):

$$\sigma = \frac{C_P}{C_P + C_Q} \times 100\% \tag{21}$$

5.2. Liquid film concentration profiles

The calculation of the molar fluxes out of the gas phase and from the liquid film into the liquid bulk also produces the concentration profiles of the components in the liquid film. An example of such a set of profiles is shown in Fig. 3. Note that these profiles were obtained at the very bottom of the column. Further up the column, different concentration levels prevail and consequently

Table 2
Base case input, process conditions and design variables

Parameter	Value
T (K)	323
$C^{in}_{O_2}$ (vol.%)	5
C^{in}_{NO} (vppm)	250
C^{out}_{NO} (vppm)	25
V_{SL} (m/s)	0.01
V_{SG} (m/s)	1
$C^{in}_{FeII(EDTA)}$ (mol/m^3)	30
$k_{G,NO}$ (m/s)	3.55×10^{-2}
k_{G,O_2} (m/s)	3.30×10^{-2}
$k_{L,NO}$ (m/s)	3.88×10^{-4}
k_{L,O_2} (m/s)	1.83×10^{-4}
a (m^2/m^3)	240
Flooding (%)	54%
ε_L	0.058

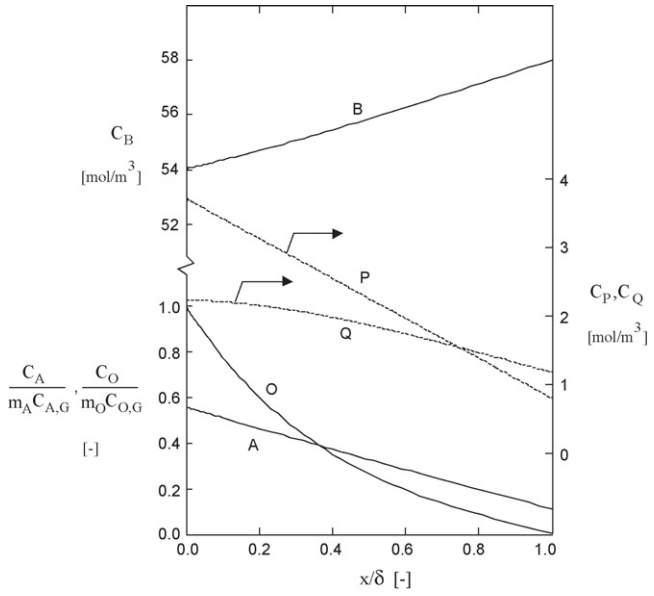

Fig. 3. Typical concentration profiles in the liquid film at $h = 0$ [m]. Base case conditions, but with $C^{in}_{Fe^{II}(EDTA)} = 60$ mol/m^3.

different profiles were obtained. Nevertheless, the profiles are typical in that the overall picture was always qualitatively similar: the concentrations of A and P varied almost linearly with the film depth because reaction (1) is reversible, instantaneous and always $C_B \gg C_A$, and the profiles of O and Q were also linear or, at most, only slightly curved because reaction (2) is only moderately fast.

In the literature, the influence of a reaction on the absorption rate of a component is often quantified using the so-called enhancement factor, E, which is defined as the ratio of the actual absorption flux to the flux that would have resulted from the same conditions but without any reaction. In this work, the enhancement factors encountered were in the range of $E_A = (0.3–8) \times 10^3$ and $E_O = 1.0–3.0$, for NO and oxygen, respectively.

In Fig. 3 the profiles of the dissolved gasses are plotted as the ratio of their concentrations to the concentrations that would be in physical equilibrium with the local gas phase concentrations. Not only does this scale the profiles nicely into the 0–1 interval, but it also illustrates another general observation. The ratio $C_O/(m_O C_{O,G})$ almost exactly equals one at the interface, indicating that the absorption of oxygen is completely liquid phase limited, with negligible gas phase resistance. The interface concentration ratio of NO, on the other hand, is much smaller than one, indicative of considerable gas phase resistance for this component.

5.3. Effect of the column temperature

Previous experimental studies in stirred cell contactors have shown that the temperature has a profound effect on the overall absorption rates of NO and oxygen. Lower temperatures favored the overall rate of NO absorption compared to the overall rate of oxygen absorption [4].

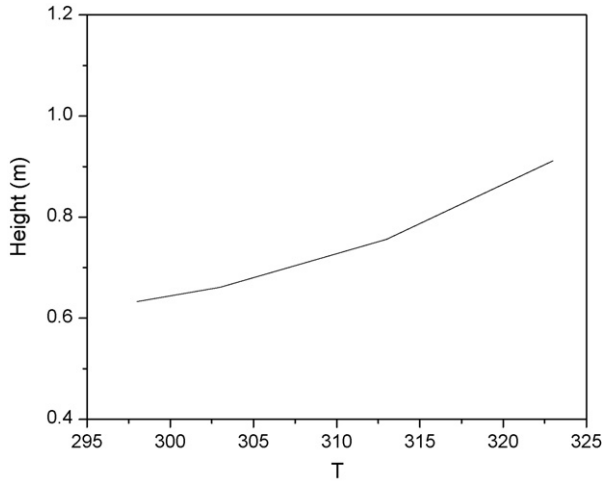

Fig. 4. Calculated column height for $\eta = 90\%$ as a function of the temperature. See Table 2 for the other conditions.

The effect of the column temperature on column performance has been modeled in the range 298–323 K. At lower temperatures, the calculated height of the packed column to achieve 90% removal efficiency decreased considerably. As shown in Fig. 4, the calculated height at 298 K is 30% lower than at 323 K. These findings are in line with earlier experimental studies in a stirred cell contactor [2], where it was shown that the overall NO absorption rate is significantly higher at lower temperatures.

The selectivity of the gas absorption, Eq. (21), is also strongly temperature dependent and increases from 45% at 328 K to 66% at 298 K, see Fig. 5. Hence, the undesired oxidation reaction is suppressed considerably at low temperatures. The pressure drops at lower temperatures are lower than the value calculated for the base case (328 K). These modeling results imply that the absorber unit should be operated at temperatures as low as possible.

5.4. Effect of the inlet $C_{FeII(EDTA)}$

The inlet $C_{FeII(EDTA)}$ has shown to be an important process variable in simultaneous absorption experiments in stirred cell

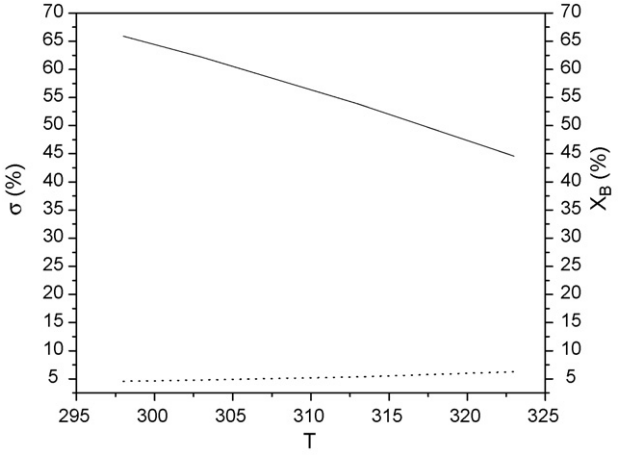

Fig. 5. Calculated σ (solid line) and X_B (dotted line) as a function of the temperature for 90% NO removal. See Table 2 for the other conditions.

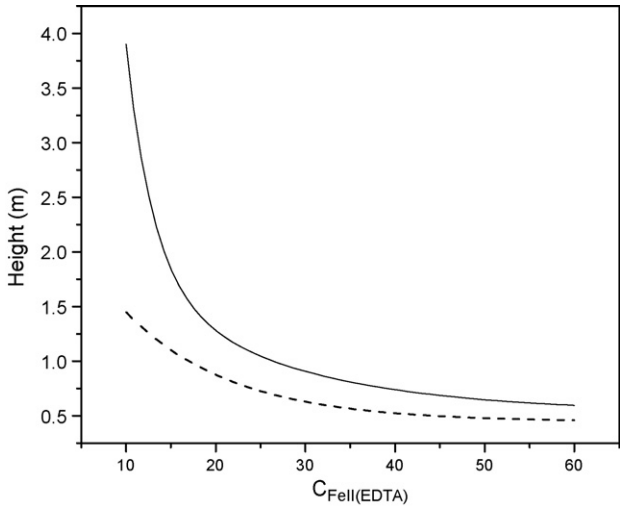

Fig. 6. Required column height for 90% removal efficiency as a function of the inlet $C_{FeII(EDTA)}$. Solid line: base case ($T = 323$ K); dashed line: $T = 298$ K. See Table 2 for other conditions.

contactors [4]. Model calculations with inlet $C_{FeII(EDTA)}$ in the range between 10 and 60 mol/m^3 were applied to study the effects on the absorption process in the packed tower reactor. All other conditions were equal to the base case as given in Table 2. The inlet $C_{FeII(EDTA)}$ has a pronounced effect on the column performance, see Fig. 6 for details. The required height of the packed tower for 90% removal efficiency is 85% lower at 60 mol/m^3 when compared to 10 mol/m^3.

The selectivity as a function of the $C_{FeII(EDTA)}$ is represented in Fig. 7. The selectivity initially increases with an increasing $C_{FeII(EDTA)}$, it reaches a maximum value for $C_{FeII(EDTA)} \approx 35$ mol/m^3 and subsequently decreases. To suppress Fe oxidation at high temperatures, it appears beneficial to work in the range of 30–40 mol/m^3. As expected, X_B decreases when the $C_{FeII(EDTA)}$ increases. X_B is only 3.4% when the highest concentration of iron chelate is applied in the simulation.

In the previous paragraph, it was shown that it is favorable to operate the column at low temperatures. The effect of the $C_{Fe(II)EDTA}$ in the inlet on column performance was also evaluated for $T = 298$ K. The results are given in Figs. 6 and 7. As expected, the required column height for 90% removal efficiency is lower when applying higher $C_{FeII(EDTA)}$ (Fig. 6). The required height at 298 K is always lower compared to 323 K, irrespective of the $C_{FeII(EDTA)}$. The selectivity of the process as a function of the $C_{Fe(II)EDTA}$ shows a different pattern at the two temperatures. At 323 K, the selectivity versus the $C_{FeII(EDTA)}$ shows an optimum at about 30–40 mol/m^3. This optimum is absent at 328 K and a small decrease of σ was observed when increasing the $C_{FeII(EDTA)}$.

5.5. Negative effect of overdesign

Simulations performed for the base case ($T = 323$ K) and a relatively low $C_{FeII(EDTA)}$ (10 mol/m^3) reveal a very remarkable feature (Fig. 8). It appears that the column efficiency lowers when the height of the column is increased beyond an optimum. This suggests that NO desorption may occur at certain conditions within the column and particularly when increasing the column length. In case the $C_{FeII(EDTA)}$ exceeds 10 mol/m^3, NO desorption was not observed. For instance, at 30 mol/m^3, efficiency drops were not observed when increasing the column height up to 12 m.

This lowering of the efficiency when using longer absorption columns in combination with low inlet Fe^{II}(EDTA) concentrations is likely the result of the mutual interactions between the reaction of Fe^{II}(EDTA) with NO and oxygen. Gambardella et al. [2] reported that the reaction between NO and $C_{FeII(EDTA}$ is an equilibrium reaction, whereas the reaction with oxygen is irreversible [3]. Both reactions occur simultaneously in the column and it is well possible that at certain conditions (high temperature and low $C_{FeII(EDTA)}$), the NO concentration in the gas phase is lower than the equilibrium value. These findings indicate that overdesign of the absorber unit may result in reduced column performance.

We can explore this peculiar behaviour by taking a closer look at the gas phase concentrations of NO and oxygen versus the

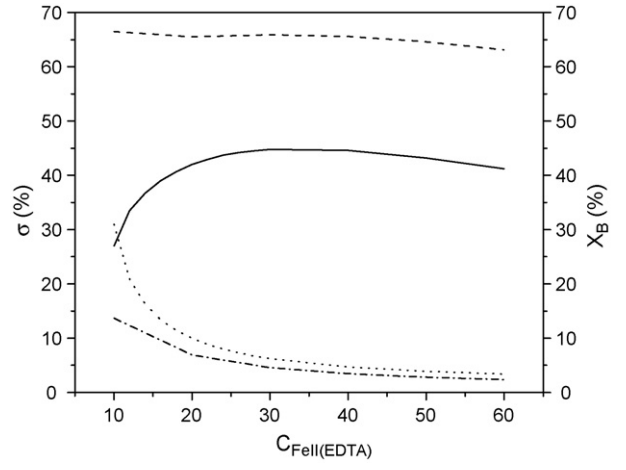

Fig. 7. σ and X_B as a function of $C_{FeII(EDTA)}$ and temperature for $\eta = 90\%$. $T = 323$ K: σ (solid line), X_B (dotted line); $T = 298$ K: σ (dashed line), X_B (dashed-dotted line). See Table 2 for the other conditions.

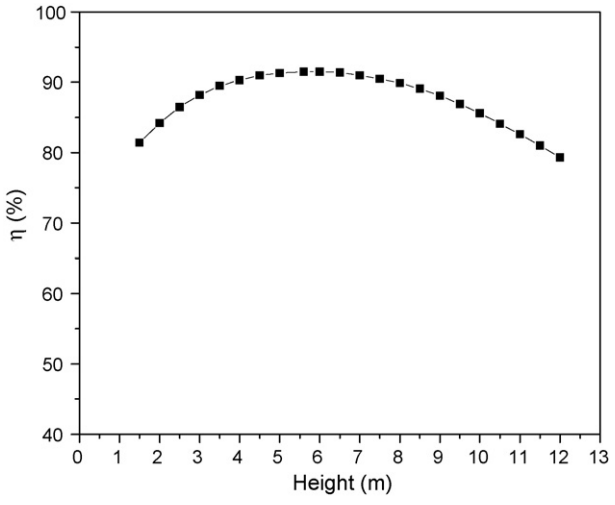

Fig. 8. Efficiency of the NO removal as a function of the reactor height. Base case with $C_{FeII(EDTA)} = 10$ mol/m^3. See Table 2 for the other conditions.

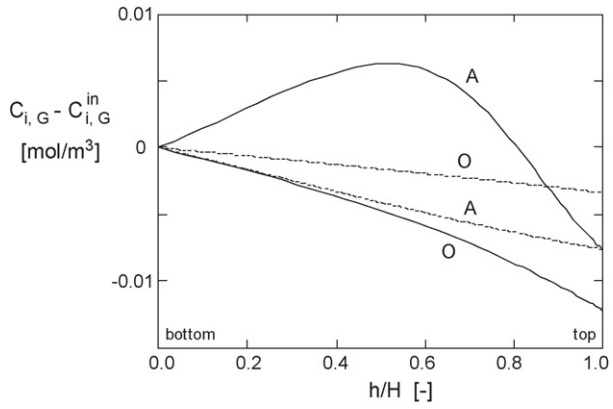

Fig. 9. Variation of the gas phase concentrations of NO (A) and oxygen (O) over the height of the packing. Base case conditions, but with $C^{in}_{Fe^{II}(EDTA)} = 10\,mol/m^3$. Solid lines: $H = 12.0$ m; dotted lines: $H = 2.3$ m.

relative height of the packing for two different packing heights with otherwise similar conditions, see Fig. 9.

The column heights were purposely chosen in such a way, i.e. at 12.0 and 2.3 m, that the NO removal efficiency is exactly the same, to illustrate the remarkable behaviour that overdesign of the absorber can result in a reduced efficiency. Although the NO concentration in the gas leaving the absorber is the same, the variation over the column height is very different. Also, the amount of oxygen absorbed in case of the 12.0 m packing height is more than three times larger as compared to the 2.3 m column. To understand the differences, a plot of the NO absorption fluxes for both cases is helpful, see Fig. 10.

In the case of the 2.3 m column, the absorption flux is always in the gas-to-liquid direction, and varies approximately in the range of $(1.0–1.5) \times 10^{-5}$ mol m^{-2} s^{-1}. As a consequence, the NO concentration in the gas phase gradually and monotonously decreases.

In case of the 12.0 m column, the amount of oxygen absorbed into the liquid is very large, which, in the lower part of the column, results in such a large conversion of Fe^{II}(EDTA) to Fe^{III}(EDTA) that the equilibrium reaction (1) is driven into the opposite direction, and desorption of NO occurs.

In the case of the 12.0 m packing, the peculiar variation of the NO flux, with two extremes (see Fig. 10), can be explained

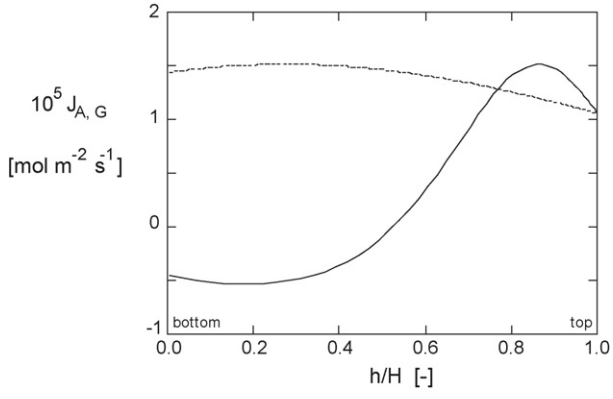

Fig. 10. Variation of the NO flux leaving the gas phase with the height of the packing. Conditions: see Fig. 9. Solid line: $H = 12.0$ m; dotted line: $H = 2.3$ m.

for example if we follow the liquid as it flows down the packing starting at the top of the column, $h/H = 1$. First the flux is positive because the almost lean liquid has not yet absorbed much oxygen, and it increases as we move down the column because the NO concentration increases resulting in a larger driving force for absorption. Going further down the packing, the increase of the NO flux drops, and is turned into a decrease below $h/H \cong 0.85$ because less and less Fe^{II}(EDTA) is available due to oxidation. Below $h/H \cong 0.55$ NO is desorbed from the liquid because the oxidation of Fe^{II}(EDTA) drives the equilibrium reaction (1) in the reverse direction and Fe^{II}(NO)(EDTA) is converted into free NO and Fe^{II}(EDTA). Below $h/H \cong 0.2$ the NO flux becomes somewhat less negative because of depletion of Fe^{II}(NO)(EDTA).

6. Conclusions

A rate based, steady state reactor model has been developed for the simultaneous absorption of NO and oxygen in an aqueous Fe^{II}(EDTA) solutions in a counter current packed column reactor at isothermal conditions. When applying typical BiodeNOx conditions ($C_{FeII(EDTA)} = 30$ mol/m^3, $T = 323$ K, $C_{NOin} = 250$ vppm, $C_{O_2 in} = 5$ vol.%) combined with superficial velocities for the liquid and gas phase of 0.01 and 1 m/s, respectively, the calculated height of the scrubber to achieve 90% NO removal efficiency is 0.91 m.

A remarkable improvement in absorber performance may be expected when operating the column at lower temperatures. Not only the required column height for 90% removal efficiency is reduced considerably, but also the overall rate of undesired oxidation reaction is significantly reduced.

Variations of the inlet $C_{FeII(EDTA)}$ at 328 K, indicate that the selectivity of the absorption process shows a maximum value (45%) at $C_{FeII(EDTA}$ between 30 and 40 mol/m^3. Lowering the temperature from 323 to 298 K results in higher selectivities (62%) and the observed maximum of the selectivity as a function of the $C_{FE(II)EDTA}$ is absent.

At certain process conditions, desorption of NO may occur, leading to a lowering of the NO removal efficiency at increasing column lengths. These findings indicate that overdesign of the absorber unit may result in reduced column performance.

References

[1] C.J. Buisman, H. Dijkman, P.L. Verbaak, A.J. Den Hartog, Process for purifying flue gas containing nitrogen oxides, US Patent no. US5891408 (1999).

[2] F. Gambardella, M.S. Alberts, J.G.M. Winkelman, H.J. Heeres, Experimental and modeling studies on the absorption of NO in aqueous ferrous EDTA solutions, Ind. Eng. Chem. Res. 44 (2005) 4242–4324.

[3] F. Gambardella, J.K. Ganzeveld, J.G.M. Winkelman, H.J. Heeres, Kinetics of the reaction of Fe^{II}(EDTA) with oxygen in aqueous solutions, Ind. Eng. Chem. Res. 44 (2005) 8190–8198.

[4] F. Gambardella, J.G.M. Winkelman, H.J. Heeres, Experimental and modeling studies on the simultaneous absorption of NO and O_2 in aqueous iron chelate solutions, Chem. Eng. Sci. 61 (2006) 6880–6891.

[5] F. Gambardella, L.M. Galan Sanchez, K.J. Ganzeveld, J.G.M. Winkelman, H.J. Heeres, Reactive NO absorption in aqueous Fe^{II}(EDTA) solutions in the presence of denitryfing microorganisms, Chem. Eng. J. 116 (2006) 67–75.

[6] K.R. Westerterp, W.P.M. van Swaaij, A.A.C.M. Beenackers, Chemical Reactor Design and Operation, Wiley and Sons, New York, 1984.
[7] T. Schneppensieper, S. Finkler, R. van Eldik, Tuning the reversible binding of NO to Iron (II) aminocarboxylate and related complexes in aqueous solution, Eur. J. Inorg. Chem. (2001) 491.
[8] S.O. Travin, Yu.I. Skurlatov, Kinetics and mechanism of the reaction of iron (II)ethylenediaminotetra-acetate (Fe^{2+} EDTA) with molecular oxygen in the presence of ligands, Russ. J. Phys. Chem. 55 (1981) 815.
[9] E. Sada, H. Kumazawa, Oxidation kinetics of Fe^{II}EDTA and Fe^{II}NTA chelates by dissolved oxygen, Ind. Eng. Chem. Res. 26 (1987) 1468.
[10] E.R. Brown, J.D. Mazzarella, Mechanism of oxidation of ferrous polydentate complexes by dioxygen, J. Electroanal. Chem. 222 (1987) 173.
[11] V. Zang, R. van Eldik, Kinetics and mechanism of the autoxidation of iron (II) induced through chelation by ethylenediaminetetraacetate and related ligands, Inorg. Chem. 29 (1990) 1705.
[12] H.J. Wubs, A.A.C.M. Beenackers, Kinetics of the oxidation of ferrous chelates of EDTA and HEDTA in aqueous solution, Ind. Eng. Chem Res. 32 (1993) 2580.
[13] D.L. Wise, G. Houghton, Diffusion coefficients of neon, krypton, xenon, carbon monoxide and nitric oxide in water at 10–60 °C, Chem. Eng. Sci. 23 (1968) 1211.
[14] L.P.B.M. Janssen, M.M.C.G. Warmoeskerken, Transport Phenomena Data Companion, Delftse Universitaire Pers, The Netherlands, 1987.
[15] C.S. Ho, L.-K. Ju, R.F. Baddour, D.I.C. Wang, Simultaneous measurements of oxygen diffusion coefficients and solubilities in electrolyte solutions with a polarographic oxygen electrode, Chem. Eng. Sci. 43 (1990) 3093–3107.
[16] G.A. O'Conner, W.L. Lindsay, S.R. Olsen, Diffusion of iron chelates in soils, Soil Sci. Soc. Am. Proc. 35 (1971) 407–410.
[17] R.C. Reid, J.M. Prausnitz, B.E. Poling, Properties of Gases and Liquids, McGraw-Hill, US, 1987.
[18] T.E. Daubert, R.D. Danner, Data Compilation Tables of Properties of Pure Compounds, AIChE, New York, 1985.
[19] K. Onda, E. Sada, Y. Okomuto, Mass transfer coefficients between gas and liquid phases in packed columns, J. Chem. Eng. Jpn. 1 (1968) 62–66.
[20] K. Onda, M. Takahashi, Y. Okumoto, Mass transfer coefficients between gas and liquid phases in packed columns, J. Chem. Eng. Jpn. 1 (1968) 56–61.
[21] P. Trambouze, H. van Landeghem, J.P. Wauquier, Chemical Reactors, Edition Technip, Paris, 1988.
[22] J.E. Buchanan, Holdup in irrigated ring-packed towers below the loading point, Ind. Eng. Chem. Fund. 6 (1967) 400–407.